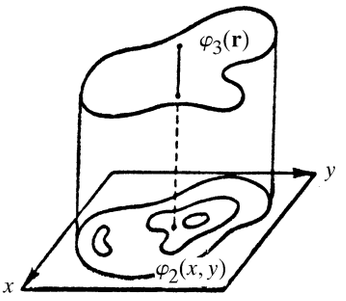

Fig. 2.5.6.1. A three-dimensional object φ_3 and its two-dimensional projection φ_2.

et al., 1968; Gordon *et al.*, 1970; Vainshtein, 1971*a*; Ramachandran & Lakshminarayanan, 1971; Vainshtein & Orlov, 1972, 1974; Gilbert, 1972*a*).

On the other hand, three-dimensional reconstruction can be carried out using the Fourier transformation, *i.e.* by transition to reciprocal space. The Fourier reconstruction is based on the well known theorem: the Fourier transformation of projection φ_2 of a three-dimensional object φ_3 is the central (*i.e.* passing through the origin of reciprocal space) two-dimensional plane cross section of a three-dimensional transform perpendicular to the projection vector (DeRosier & Klug, 1968; Crowther, DeRosier & Klug, 1970; Bracewell, 1956). In Cartesian coordinates a three-dimensional transform is

$$\mathscr{F}_3[\varphi_3(\mathbf{r})] = \Phi_3(uvw) = \iiint \varphi_3(xyz) \times \exp\{2\pi i(ux + vy + wz)\}\ \mathrm{d}x\ \mathrm{d}y\ \mathrm{d}z. \quad (2.5.6.3)$$

The transform of projection $\varphi_2(xy)$ along z is

$$\begin{aligned}\mathscr{F}_2[\varphi_2(xy)] &= \Phi_3(uv0) = \iiint \varphi_3(xyz) \times \exp\{2\pi i(ux + vy + 0z)\}\ \mathrm{d}x\ \mathrm{d}y\ \mathrm{d}z \\ &= \iiint \varphi_3(xyz)\ \mathrm{d}z \exp\{2\pi i(ux + vy)\}\ \mathrm{d}x\ \mathrm{d}y \\ &= \iint \varphi_2(xy) \exp\{2\pi i(ux + vy)\}\ \mathrm{d}x\ \mathrm{d}y \\ &= \Phi_2(uv). \end{aligned} \quad (2.5.6.4)$$

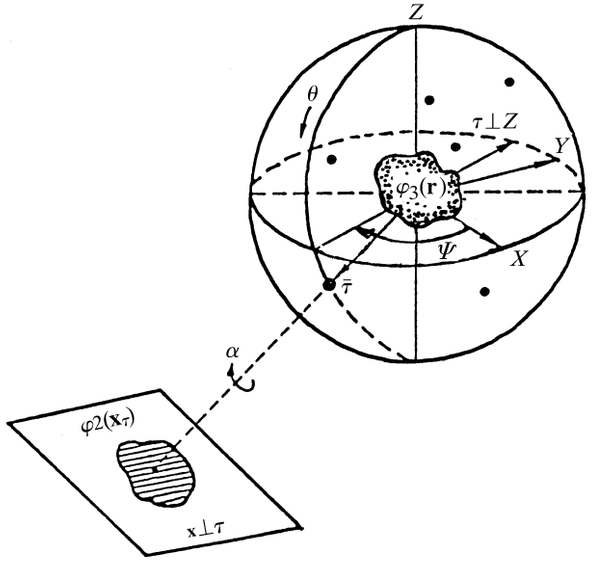

Fig. 2.5.6.2. The projection sphere and projection φ_2 of φ_3 along $\boldsymbol{\tau}$ onto the plane $\mathbf{x} \perp \boldsymbol{\tau}$. The case $\boldsymbol{\tau} \perp z$ represents orthoaxial projection. Points indicate a random distribution of $\boldsymbol{\tau}$.

In the general case (2.5.6.1) of projecting the plane $\mathbf{x}(xy) \| \mathbf{u}(uv) \perp \boldsymbol{\tau}$ along the vector $\boldsymbol{\tau}$

$$\mathscr{F}_2[\varphi_2(\mathbf{x}_\tau)] = \Phi_2(\mathbf{u}_\tau). \quad (2.5.6.5)$$

Reconstruction with Fourier transformation involves transition from projections φ_{2i} at various $\boldsymbol{\tau}_i$ to cross sections Φ_{2i}, then to construction of the three-dimensional transform $\Phi_3(\mathbf{u})$ by means of interpolation between φ_{2i} in reciprocal space, and transition by the inverse Fourier transformation to the three-dimensional distribution $\varphi_3(\mathbf{r})$:

$$\begin{aligned}&\text{set } \varphi_{2i}(\mathbf{x}_{\tau i}) \rightarrow \text{ set } \mathscr{F}_2(\varphi_2) \\ &\quad \equiv \text{ set } \Phi_{2i} \rightarrow \Phi_3 \rightarrow \mathscr{F}_3^{-1}(\Phi_3) \equiv \varphi_3(\mathbf{r}). \end{aligned} \quad (2.5.6.6)$$

Transition (2.5.6.2) or (2.5.6.6) from two-dimensional electron-microscope images (projections) to a three-dimensional structure allows one to consider the complex of methods of 3D reconstruction as three-dimensional electron microscopy. In this sense, electron microscopy is an analogue of methods of structure analysis of crystals and molecules providing their three-dimensional spatial structure. But in structure analysis with the use of X-rays, electrons, or neutrons the initial data are the data in reciprocal space $|\Phi_{2i}|$ in (2.5.6.6), while in electron microscopy this role is played by two-dimensional images $\varphi_{2i}(\mathbf{x})$ [(2.5.6.2), (2.5.6.6)] in real space.

In electron microscopy the 3D reconstruction methods are, mainly, used for studying biological structures (symmetric or asymmetric associations of biomacromolecules), the quaternary structure of proteins, the structures of muscles, spherical and rod-like viruses, bacteriophages, and ribosomes.

An exact reconstruction is possible if there is a continuous set of projections φ_τ corresponding to the motion of the vector $\boldsymbol{\tau}(\theta, \psi)$ over any continuous line connecting the opposite points on the unit sphere (Fig. 2.5.6.2). This is evidenced by the fact that, in this case, the cross sections $\mathscr{F}_2$ which are perpendicular to $\boldsymbol{\tau}$ in Fourier space (2.5.6.4) continuously fill the whole of its volume, *i.e.* give $\mathscr{F}_3(\varphi_3)$ (2.5.6.3) and thereby determine $\varphi_3(\mathbf{r}) = \mathscr{F}^{-1}(\Phi_3)$.

In reality, we always have a discrete (but not continuous) set of projections φ_{2i}. The set of φ_{2i} is, practically, obtained by the rotation of the specimen under the beam through various angles (Hoppe & Typke, 1979) or by imaging of the objects which are randomly oriented on the substrate at different angles (Kam, 1980; Van Heel, 1984). If the object has symmetry, one of its projections is equivalent to a certain number of different projections.

The object $\varphi_3(\mathbf{r})$ is finite in space. For function $\varphi_3(\mathbf{r})$ and any of its projections there holds the normalization condition

$$\Omega = \int \varphi_3(\mathbf{r})\ \mathrm{d}v_\mathbf{r} = \int \varphi_2(\mathbf{x})\ \mathrm{d}\mathbf{x} = \int \varphi_1(x)\ \mathrm{d}x, \quad (2.5.6.7)$$

where Ω is the total 'weight' of the object described by the density distribution φ_3. If one assumes that the density of an object is constant and that inside the object $\varphi = \text{constant} = 1$, and outside it $\varphi = 0$, then Ω is the volume of an object. The volume of an object, say, of molecules, viruses and so on, is usually known from data on the density or molecular mass.

2.5.6.2. *Orthoaxial projection*

In practice, an important case is where all the projection directions are orthogonal to a certain straight line: $\boldsymbol{\tau} \perp z$ (Fig. 2.5.6.3). Here the axis of rotation or the axis of symmetry of an object is perpendicular to an electron beam. Then the three-dimensional problem is reduced to the two-dimensional one, since each cross section $\varphi_{2i}(\mathbf{x}, z = \text{constant})$ is represented by its one-dimensional projections. The direction of vector $\boldsymbol{\tau}$ is defined by the rotational angle ψ of a specimen:

$$\varphi_1(x_{\psi_i}) \equiv L^i(\psi_i) = \int \varphi_2(\mathbf{x})\ \mathrm{d}\tau_\psi;\ x_i \perp \boldsymbol{\tau}_\psi. \quad (2.5.6.8)$$

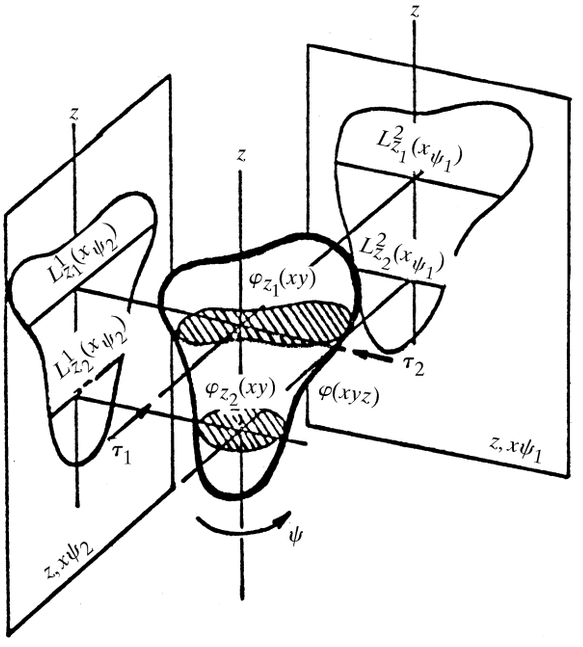

Fig. 2.5.6.3. Orthoaxial projection.

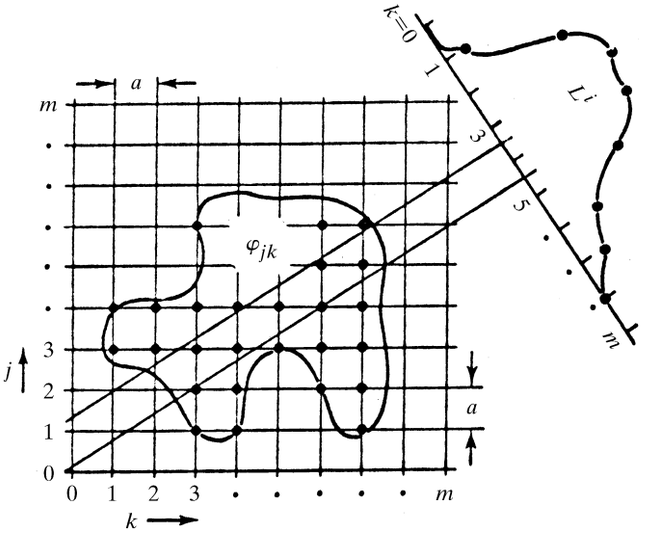

Fig. 2.5.6.4. Discretization and oblique projection.

In this case, the reconstruction is carried out separately for each level z_l:

$$\text{set } \varphi_{1,\,z_l}(x_\psi) \equiv \text{ set } L^i_{z_l} \rightarrow \varphi_{2i}(xyz_l) \qquad (2.5.6.9)$$

and the three-dimensional structure is obtained by superposition of layers $\varphi_{2z_l}(xy)\Delta z$ (Vainshtein *et al.*, 1968; Vainshtein, 1978).

2.5.6.3. *Discretization*

In direct methods of reconstruction as well as in Fourier methods the space is represented as a discrete set of points $\varphi(\mathbf{x}_{jk})$ on a two-dimensional net or $\varphi(\mathbf{r}_{jkl})$ on a three-dimensional lattice. It is sometimes expedient to use cylindrical or spherical coordinates. In two-dimensional reconstruction the one-dimensional projections are represented as a set of discrete values L^i, at a certain spacing in x_ψ. The reconstruction (2.5.6.9) is carried out over the discrete net with m^2 nodes φ_{jk}. The net side A should exceed the diameter of an object D, $A > D$; the spacing $a = A/m$. Then (2.5.6.8) transforms into the sum

$$L^i = \sum_k \varphi_{jk}. \qquad (2.5.6.10)$$

For oblique projections the above sum is taken over all the points within the strips of width a along the axis $\boldsymbol{\tau}_{\psi_i}$ (Fig. 2.5.6.4).

The resolution δ of the reconstructed function depends on the number h of the available projections. At approximately uniform angular distribution of projections, and diameter equal to D, the resolution at reconstruction is estimated as

$$\delta \simeq 2D/h. \qquad (2.5.6.11)$$

The reconstruction resolution δ should be equal to or somewhat better than the instrumental resolution d of electron micrographs ($\delta < d$), the real resolution of the reconstructed structure being d. If the number of projections h is not sufficient, *i.e.* $\delta > d$, then the resolution of the reconstructed structure is δ (Crowther, DeRosier & Klug, 1970; Vainshtein, 1978).

In electron microscopy the typical instrumental resolution d of biological macromolecules for stained specimens is about 20 Å; at the object with diameter $D \simeq 200$ Å the sufficient number h of projections is about 20. If the projections are not uniformly distributed in projection angles, the resolution decreases towards $\mathbf{x} \perp \boldsymbol{\tau}$ for such $\boldsymbol{\tau}$ in which the number of projections is small.

Properties of projections of symmetric objects. If the object has an N-fold axis of rotation, its projection has the same symmetry. At orthoaxial projection perpendicular to the N-fold axis the projections which differ in angle at $j(2\pi/N)$ are identical:

$$\varphi_2(\mathbf{x}_\psi) = \varphi_2[\mathbf{x}_{\psi + j(2\pi/N)}] \quad (j = 1, 2, \ldots, N). \qquad (2.5.6.12)$$

This means that one of its projections is equivalent to N projections. If we have h independent projections of such a structure, the real number of projections is hN (Vainshtein, 1978). For a structure with cylindrical symmetry ($N = \infty$) one of its projections fully determines the three-dimensional structure.

Many biological objects possess helical symmetry – they transform into themselves by the screw displacement operation $s_{p/q}$, where p is the number of packing units in the helical structure per q turns of the continuous helix. In addition, the helical structures may also have the axis of symmetry N defining the pitch of the helix. In this case, a single projection is equivalent to $h = pN$ projections (Cochran *et al.*, 1952).

Individual protein molecules are described by point groups of symmetry of type N or $N/2$. Spherical viruses have icosahedral symmetry 532 with two-, three- and fivefold axes of symmetry. The relationship between vectors $\boldsymbol{\tau}$ of projections is determined by the transformation matrix of the corresponding point group (Crowther, Amos *et al.*, 1970).

2.5.6.4. *Methods of direct reconstruction*

Modelling. If several projections are available, and, especially, if the object is symmetric, one can, on the basis of spatial imagination, recreate approximately the three-dimensional model of the object under investigation. Then one can compare the projections of such a model with the observed projections, trying to draw them as near as possible. In early works on electron microscopy of biomolecules the tentative models of spatial structure were constructed in just this way; these models provide, in the case of the quaternary structure of protein molecules or the structure of viruses, schemes for the arrangement of protein subunits. Useful subsidiary information in this case can be obtained by the method of optical diffraction and filtration.

2.5.6.5. *The method of back-projection*

This method is also called the synthesis of projection functions. Let us consider a two-dimensional case and stretch along τ_{ψ_i} each one-dimensional projection L^i (Fig. 2.5.6.5) by a certain length b; thus, we obtain the projection function

$$L^i(\mathbf{x}) = \frac{1}{b} L^i(x_i) \cdot 1(\tau_i). \tag{2.5.6.13}$$

Let us now superimpose h functions L^i

$$\sum_{i=1}^{h} L^i(\mathbf{x}) = \Sigma_2(\mathbf{x}). \tag{2.5.6.14}$$

The continuous sum over the angles of projection synthesis is

$$\Sigma_2(\mathbf{x}) = \int_0^{\pi} L(\psi, \mathbf{x})\, \mathrm{d}\psi = \rho_2(\mathbf{x}) * |\mathbf{x}|^{-1}$$

$$\simeq \sum_{i=1}^{h} L^i = \rho_2(\mathbf{x}) + B(1); \tag{2.5.6.15}$$

this is the convolution of the initial function with a rapidly falling function $|\mathbf{x}|^{-1}$ (Vainshtein, 1971*b*). In (2.5.6.15), the approximation for a discrete set of h projections is also written. Since the function $|\mathbf{x}|^{-1}$ approaches infinity at $x = 0$, the convolution with it will reproduce the initial function $\rho(\mathbf{x})$, but with some background B decreasing around each point according to the law $|\mathbf{x}|^{-1}$. At orthoaxial projection the superposition of cross sections $\varphi_2(\mathbf{x}, z_k)$ arranged in a pile gives the three-dimensional structure φ_3.

Radon operator. Radon (1917; see also Deans, 1983) gave the exact solution of the problem of reconstruction. However, his mathematical work was for a long time unknown to investigators engaged in reconstruction of a structure from images; only in the early 1970s did some authors obtain results analogous to Radon's (Ramachandran & Lakshminarayanan, 1971; Vainshtein & Orlov, 1972, 1974; Gilbert, 1972*a*).

The convolution in (2.5.6.15) may be eliminated using the Radon integral operator, which modifies projections by introducing around each point the negative values which annihilate on superposition the positive background values. The one-dimensional projection modified with the aid of the Radon operator has the form

$$\tilde{L}(x_\psi) = \frac{1}{2\pi^2} \int_0^{\infty} \frac{2L(x_\psi) - L(x_\psi + x'_\psi) - L(x_\psi - x'_\psi)}{x'^2_\psi}\, \mathrm{d}x'_\psi. \tag{2.5.6.16}$$

Now $\varphi_2(\mathbf{x})$ is calculated analogously to (2.5.6.14), not from the initial projections L but from the modified projection $\tilde{L}$:

$$\varphi_2(\mathbf{x}) = \int_0^{\pi} \tilde{L}(\psi, \mathbf{x})\, \mathrm{d}\psi \simeq \sum_{i=1}^{k} \tilde{L}_i(\psi_i, \mathbf{x}). \tag{2.5.6.17}$$

The reconstruction of high-symmetry structures, in particular helical ones, by the direct method is carried out from one projection making use of its equivalence to many projections. The Radon formula in discrete form can be obtained using the double Fourier transformation and convolution (Ramachandran & Lakshminarayanan, 1971).

2.5.6.6. *The algebraic and iteration methods*

These methods have been derived for the two-dimensional case; consequently, they can also be applied to three-dimensional reconstruction in the case of orthoaxial projection.

Let us discretize $\varphi_2(\mathbf{x})$ by a net m^2 of points φ_{jk}; then we can construct the system of equations (2.5.6.10).

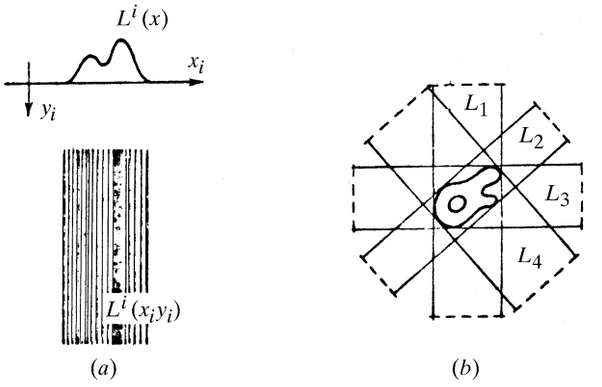

Fig. 2.5.6.5. (*a*) Formation of a projection function; (*b*) superposition of these functions.

When h projections are available the condition of unambiguous solution of system (2.5.6.10) is: $h \geq m$. At $m \simeq (3\text{–}5)h$ we can, in practice, obtain sufficiently good results (Vainshtein, 1978).

Methods of reconstruction by iteration have also been derived that cause some initial distribution to approach one $\varphi_2(\mathbf{x})$ satisfying the condition that its projection will resemble the set L^i. Let us assign on a discrete net φ_{jk} as a zero-order approximation the uniform distribution of mean values (2.5.6.7)

$$\varphi^0_{jk} = \langle \varphi \rangle = \Omega / m^2. \tag{2.5.6.18}$$

The projection of the qth approximation φ^q_{jk} at the angle φ_i (used to account for discreteness) is L^{iq}_n.

The next approximation φ^{q+1} for each point jk is given in the method of 'summation' by the formula

$$\varphi^{q+1}_{jk} = \max[\varphi^q_{jk} + (L^i_n - L^{i,q}_n)/N^i_{L_n};\, 0], \tag{2.5.6.19}$$

where N_{L^i} is the number of points in a strip of the projection L^i_n. One cycle of iterations involves running φ^q_{jk} around all of the angles ψ_j (Gordon *et al.*, 1970).

When carrying out iterations, we may take into account the contribution not only of the given projection, but also of all others. In this method the process of convergence improves. Some other iteration methods have been elaborated (Gordon & Herman, 1971; Gilbert, 1972*b*; Crowther & Klug, 1974; Gordon, 1974).

2.5.6.7. *Reconstruction using Fourier transformation*

This method is based on the Fourier projection theorem [(2.5.6.3)–(2.5.6.5)]. The reconstruction is carried out according to scheme (2.5.6.6) (DeRosier & Klug, 1968; Crowther, DeRosier & Klug, 1970; Crowther, Amos *et al.* 1970; DeRosier & Moore, 1970; Orlov, 1975). The three-dimensional Fourier transform $\mathscr{F}_3(\mathbf{u})$ is found from a set of two-dimensional cross sections $\mathscr{F}_2(\mathbf{u})$ on the basis of the Whittaker–Shannon interpolation. If the object has helical symmetry (which often occurs in electron microscopy of biological objects, *e.g.* on investigating bacteriophage tails, muscle proteins) cylindrical coordinates are used. Diffraction from such structures with c periodicity and scattering density $\varphi(r, \psi, z)$ is defined by the Fourier–Bessel transform:

$$\Phi(R, \Psi, Z) = \sum_{n=-\infty}^{+\infty} \exp\left[in\left(\Psi + \frac{\pi}{2}\right)\right] \int_0^{\infty} \int_0^{2\pi} \int_0^{l} \varphi(r, \psi, z)$$

$$\times J_n(2\pi r R) \exp[-i(n\psi + 2\pi z Z)] r\, \mathrm{d}r\, \mathrm{d}\psi\, \mathrm{d}z$$

$$= \sum_n G_n(R, Z) \exp\left[in\left(\Psi + \frac{\pi}{2}\right)\right]. \tag{2.5.6.20}$$

The inverse transformation has the form

$$\rho(r,\psi,z)=\sum_n \int g_n(r,Z)\exp(in\psi)\exp(2\pi izZ)\ \mathrm{d}Z, \qquad (2.5.6.21)$$

so that g_n and G_n are the mutual Bessel transforms

$$G_n(R,Z)=\int_0^\infty g_n(rZ)J_n(2\pi rR)2\pi r\ \mathrm{d}r \qquad (2.5.6.22)$$

$$g_n(r,Z)=\int_0^\infty G_n(R,Z)J_n(2\pi rR)2\pi R\ \mathrm{d}R. \qquad (2.5.6.23)$$

Owing to helical symmetry, (2.5.6.22), (2.5.6.23) contain only those of the Bessel functions which satisfy the selection rule (Cochran *et al.*, 1952)

$$l=mp+(nq/N), \qquad (2.5.6.24)$$

where N, q and p are the helix symmetry parameters, $m=0,\pm1,\pm2,\ldots$. Each layer l is practically determined by the single function J_n with the lowest n; the contribution of other functions is neglected. Thus, the Fourier transformation of one projection of a helical structure, with an account of symmetry and phases, gives the three-dimensional transform (2.5.6.23). We can introduce into this transform the function of temperature-factor type filtering the 'noise' from large spatial frequencies.

2.5.6.8. *Three-dimensional reconstruction in the general case*

In the general case of 3D reconstruction $\varphi_3(\mathbf{r})$ from projections $\varphi_2(\mathbf{x}_\tau)$ the projection vector $\boldsymbol{\tau}$ occupies arbitrary positions on the projection sphere (Fig. 2.5.6.2). Then, as in (2.5.6.15), we can construct the three-dimensional spatial synthesis. To do this, let us transform the two-dimensional projections $\varphi_{2i}[\mathbf{x},\boldsymbol{\tau}(\theta,\psi)_i]$ by extending them along $\boldsymbol{\tau}$ as in (2.5.6.13) into three-dimensional projection functions $\varphi_3(\mathbf{r}_{\tau_i})$.

Analogously to (2.5.6.15), such a three-dimensional synthesis is the integral over the hemisphere (Fig. 2.5.6.2)

$$\begin{aligned}\Sigma_3(\mathbf{r})&=\int_\omega \varphi_3(\mathbf{r},\boldsymbol{\tau}_i)\ \mathrm{d}\omega_\tau=\varphi(\mathbf{r})*|\mathbf{r}|^{-2}\\ &\simeq \Sigma\varphi_{3i}[\mathbf{r}_{\tau(\theta,\psi)_i}]\simeq\varphi_3(\mathbf{r})+B; \qquad (2.5.6.25)\end{aligned}$$

this is the convolution of the initial function with $|\mathbf{r}|^{-2}$ (Vainshtein, 1971*b*).

To obtain the exact reconstruction of $\varphi_3(\mathbf{r})$ we find, from each $\varphi_2(\mathbf{x}_{\boldsymbol{\tau}})$, the modified projection (Vainshtein & Orlov, 1974; Orlov, 1975)

$$\tilde{\varphi}_2(\mathbf{x}_\tau)=\int\frac{\varphi_2(\mathbf{x}_{\boldsymbol{\tau}})-\varphi_2(\mathbf{x}'_{\boldsymbol{\tau}})}{|\mathbf{x}_{\boldsymbol{\tau}}-\mathbf{x}'_{\boldsymbol{\tau}}|^3}\ \mathrm{d}s_{\mathbf{x}'}. \qquad (2.5.6.26)$$

By extending $\varphi_2(\mathbf{x}_{\boldsymbol{\tau}})$ along $\boldsymbol{\tau}$ we transform them into $\tilde{\varphi}_3(\mathbf{r}_{\boldsymbol{\tau}})$. Now the synthesis over the angles $\omega_\tau=(\theta,\psi,\alpha)_\tau$ gives the three-dimensional function

$$\varphi_3(\mathbf{r})=\frac{1}{4\pi^3}\int\tilde{\varphi}_3(\mathbf{r}_{\boldsymbol{\tau}})\ \mathrm{d}\omega_{\boldsymbol{\tau}}\simeq\sum_i\tilde{\varphi}_{3i}[\mathbf{r}_{\tau(\theta,\psi,\alpha)_i}]. \qquad (2.5.6.27)$$

The approximation for a discrete set of angles is written on the right. In this case we are not bound by the coaxial projection condition which endows the experiment with greater possibilities; the use of object symmetry also profits from this. To carry out the 3D reconstruction (2.5.6.25) or (2.5.6.27) one should know all three Euler's angles ψ, θ, α (Fig. 2.5.6.2).

The projection vectors $\boldsymbol{\tau}_i$ should be distributed more or less uniformly over the sphere (Fig. 2.5.6.2). This can be achieved by using special goniometric devices.

Another possibility is the investigation of particles which, during the specimen preparation, are randomly oriented on the substrate. This, in particular, refers to asymmetric ribosomal particles. In this case the problem of determining these orientations arises.

The method of spatial correlation functions may be applied if a large number of projections with uniformly distributed projection directions is available (Kam, 1980). The space correlation function is the averaged characteristic of projections over all possible directions which is calculated from the initial projections or the corresponding sections of the Fourier transform. It can be used to find the coefficients of the object density function expansion over spherical harmonics, as well as to carry out the 3D reconstruction in spherical coordinates.

Another method (Van Heel, 1984) involves the statistical analysis of image types, subdivision of images into several classes and image averaging inside the classes. Then, if the object is rotated around some axis, the 3D reconstruction is carried out by the iteration method.

If such a specimen is inclined at a certain angle with respect to the beam, then the images of particles in the preferred orientation make a series of projections inclined at an angle β and having a random azimuth. The azimuthal rotation is determined from the image having zero inclination.

If particles on the substrate have a characteristic shape, they may acquire a preferable orientation with respect to the substrate, their azimuthal orientation α being random (Radermacher *et al.*, 1987).

In the general case, the problem of determining the spatial orientations of randomly distributed identical three-dimensional particles $\varphi_3(\mathbf{r})$ with an unknown structure may be solved by measuring their two-dimensional projections $p(\mathbf{x}_\tau)$ (Fig. 2.5.6.1)

$$p(\mathbf{x}_{\tau_i})\equiv\varphi_2(\mathbf{x}_{\tau_i})\simeq\int\varphi_3(\mathbf{r})\ \mathrm{d}\tau_i\quad\mathbf{x}\perp\boldsymbol{\tau}_i; \qquad (2.5.6.1a)$$

if the number i of such projections is not less than three, $i\geq3$ (Vainshtein & Goncharov, 1986*a*,*b*; Goncharov *et al.* 1987; Goncharov, 1987). The direction of the vector $\boldsymbol{\tau}_i$ along which the projection $p(\boldsymbol{\tau}_i)$ is obtained is set by the angle $\omega_i(\theta_i,\psi_i)$ (Fig. 2.5.6.2).

The method is based on the analysis of one-dimensional projections q_α of two-dimensional projections $p(\mathbf{x}_{\tau_i})$

$$q(x_{\perp\alpha})=\int p(\mathbf{x}_{\tau_i})\ \mathrm{d}x_{\parallel\alpha}, \qquad (2.5.6.28)$$

where α is the angle of the rotation about vector $\boldsymbol{\tau}$ in the p plane.

Lemma 1. Any two projections $p_1(\mathbf{x}_{\tau_i})$ and $p_2(\mathbf{x}_{\tau_2})$ (Fig. 2.5.6.6) have common (identical) one-dimensional projections $q_{12}(x_{12})$:

$$q_{12}(x_{12})=q_{1,\alpha_1 j}(x_{\perp\alpha_1 j})=q_{2,\alpha_2 k}(x_{\perp\alpha_2 k}). \qquad (2.5.6.29)$$

Vectors $\boldsymbol{\tau}_1$ and $\boldsymbol{\tau}_2$ (Fig. 2.5.6.3) determine plane h in which they are both lying. Vector $m_{12}=\langle\tau_1\tau_2\rangle$ is normal to plane h and parallel to axis x_{12} of the one-dimensional projection q_{12}; both $x_{\perp\alpha_1 j}$ and $x_{\perp\alpha_2 j}$ axes along which the projections q_1 and q_2 are constructed are perpendicular to x_{12}.

The corresponding lemma in the Fourier space states:

Lemma 2. Any two plane transforms, $\Phi_2(\mathbf{u}_{\tau_1})=\mathscr{F}_2 p_1$ and $\Phi_2(\mathbf{u}_{\tau_2})=\mathscr{F}_2 p_2$ intersect along the straight line v_{12} (Fig. 2.5.6.7); the one-dimensional transform $Q(v_{12})$ is the transform of $q_{12}: Q(v_{12})=\mathscr{F}_1 g_{12}$.

Thus in order to determine the orientations $\omega_i(\theta_i,\psi_i,\alpha_i)$ of a three-dimensional particle $\varphi_{3,\omega_i}(\mathbf{r})$ it is necessary either to use projections p_i in real space or else to pass to the Fourier space (2.5.6.5).

Now consider real space. The projections p_i are known and can be measured but angles α_{ij} of their rotation about vector $\boldsymbol{\tau}_i$ (Fig. 2.5.6.8) are unknown and should be determined. Let us choose any two projections p_1 and p_2 and construct a set of one-dimensional projections $q_{1,\alpha_1 j}$ and $q_{2,\alpha_2 k}$ by varying angles α_{1j} and α_{2k}. In

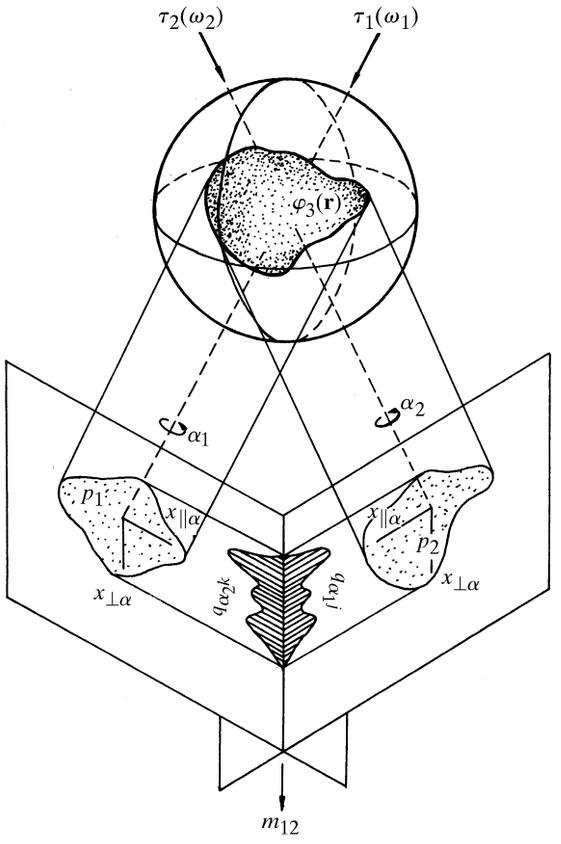

Fig. 2.5.6.6. Relative position of the particle and planes of projection.

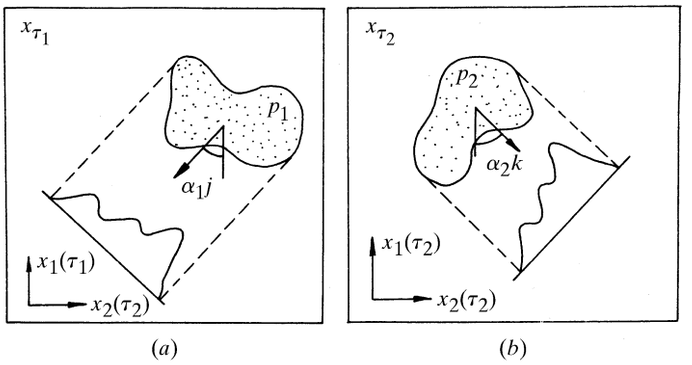

Fig. 2.5.6.8. Plane projections of a three-dimensional body. The systems of coordinates in planes (*a*) and (*b*) are chosen independently of one another.

accordance with *Lemma* 1, there exists a one-dimensional projection, common for both p_1 and p_2, which determines angles α_{1j} and α_{2k} along which p_1 and p_2 should be projected for obtaining the identical projection q_{12} (Fig. 2.5.6.5). Comparing $q_{1,\,\alpha_1 j}$ and $q_{2,\,\alpha_2 k}$ and using the minimizing function

$$D(1,2) = |q_{1,\,\alpha_1 j} - q_{2,\,\alpha_2 k}|^2 \qquad (2.5.6.30)$$

it is possible to find such a common projection q_{12}. (A similar consideration in Fourier space yields Q_{12}.)

The mutual spatial orientations of any three non-coplanar projection vectors $\boldsymbol{\tau}_1$, $\boldsymbol{\tau}_2$, $\boldsymbol{\tau}_3$ can be found from three different two-dimensional projections p_1, p_2 and p_3 by comparing the following pairs of projections: p_1 and p_2, p_1 and p_3, and p_2 and p_3, and by determining the corresponding q_{12}, q_{13} and q_{23}. The determination of angles ω_1, ω_2 and ω_3 reduces to the construction of a trihedral angle formed by planes h_{12}, h_{13} and h_{23}. Then the projections $p_i(\omega_i)$ with the known ω_i $(i = 1, 2, 3)$ can be complemented with other projections $(i = 4, 5, \ldots)$ and the corresponding values of ω can be determined. Having a sufficient number of projections and knowing the orientations ω_i, it is possible to carry out the 3D reconstruction of the object [see (2.5.6.27); Orlov, 1975; Vainshtein & Goncharov, 1986*a*; Goncharov *et al.*, 1987].

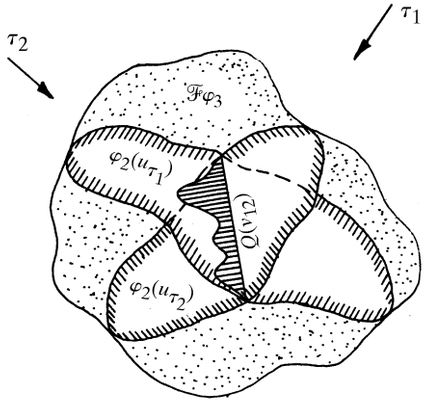

Fig. 2.5.6.7. Section of a three-dimensional Fourier transform of the density of the particles, corresponding to plane projections of this density.

2.5.7. Direct phase determination in electron crystallography (D. L. DORSET)

2.5.7.1. *Problems with 'traditional' phasing techniques*

The concept of using experimental electron-diffraction intensities for quantitative crystal structure analyses has already been presented in Section 2.5.4. Another aspect of quantitative structure analysis, employing high-resolution images, has been presented in Sections 2.5.5 and 2.5.6. That is to say, electron micrographs can be regarded as an independent source of crystallographic phases.

Before direct methods (Chapter 2.2) were developed as the standard technique for structure determination in small-molecule X-ray crystallography, there were two principal approaches to solving the crystallographic phase problem. First, 'trial and error' was used, finding some means to construct a reasonable model for the crystal structure *a priori*, *e.g.* by matching symmetry properties shared by the point group of the molecule or atomic cluster and the unit-cell space group. Secondly, the autocorrelation function of the crystal, known as the Patterson function (Chapter 2.3), was calculated (by the direct Fourier transform of the available intensity data) to locate salient interatomic vectors within the unit cell.

The same techniques had been used for electron-diffraction structure analysis (nowadays known as *electron crystallography*). In fact, advocacy of the first method persists. Because of the perturbations of diffracted intensities by multiple-beam dynamical scattering (Chapter 5.2), it has often been suggested that trial and error be used to construct the scattering model for the unit crystal in order to test its convergence to observed data after simulation of the scattering events through the crystal. This indirect approach assumes that no information about the crystal structure can be obtained directly from observed intensity data. Under more favourable scattering conditions nearer to the kinematical approximation, *i.e.* for experimental data from thin crystals made up of light atoms, trial and error modelling, simultaneously minimizing an atom–atom nonbonded potential function with the crystal-

references